Title: Energy starvation in *Daphnia magna* from exposure to a lithium cobalt oxide nanomaterial

Authors: Nicholas J Niemuth[1], Becky J Curtis[1], Elizabeth D Laudadio[2], Jelena Sostare[3], Evan A Bennett[1], Nicklaus J Neureuther[1], Aurash A Mohaimani[1], Angela Schmoldt[1], Eric D Ostovich[1], Mark R Viant[3], Robert J Hamers[2], Rebecca D Klaper[1]*

[1] School of Freshwater Sciences, University of Wisconsin-Milwaukee, 600 E Greenfield Ave., Milwaukee, WI 53204

[2] Department of Chemistry, University of Wisconsin-Madison, 1101 University Ave., Madison, WI 53706

[3]School of Biosciences, University of Birmingham, Edgbaston, Birmingham, B15 2TT, UK

* Corresponding author: rklaper@uwm.edu

Keywords: nanomaterial, nanotoxicology, metal oxide, *Daphnia magna*, next-generation sequencing, metabolomics, lithium cobalt oxide nanomaterial

Table of contents graphic

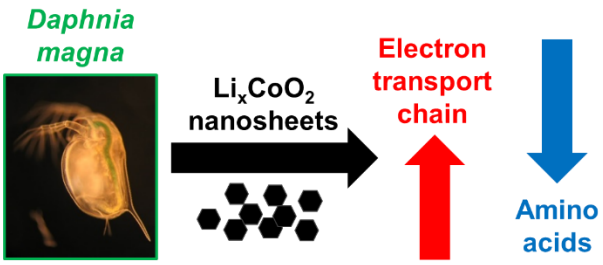

Abstract. Growing evidence across organisms points to altered energy metabolism as an adverse outcome of metal oxide nanomaterial toxicity, with a mechanism of toxicity potentially related to the redox chemistry of processes involved in energy production. Despite this evidence, the significance of this mechanism has gone unrecognized in nanotoxicology due to the field's focus on oxidative stress as a universal—but non-specific—nanotoxicity mechanism. To further explore metabolic impacts, we determined LCO's effects on these pathways in the model organism *Daphnia magna* through global gene expression analysis using RNA-Seq and untargeted metabolomics by direct-injection mass spectrometry. Our results show a sublethal 1 mg/L 48 h exposure of *D. magna* to LCO nanosheets causes significant impacts on metabolic pathways versus untreated controls, while exposure to ions released over 48 hr does not. Specifically, transcriptomic analysis using DAVID indicated significant enrichment (Benjamini-adjusted $p \leq 0.0.5$) in LCO-exposed animals for changes in pathways involved in the cellular response to starvation (25 genes), mitochondrial function (70 genes), ATP-binding (70 genes), oxidative phosphorylation (53 genes), NADH dehydrogenase activity (12 genes), and protein biosynthesis (40 genes). Metabolomic analysis using MetaboAnalyst indicated significant enrichment (gamma-adjusted $p < 0.1$) for changes in amino acid metabolism (19 metabolites) and starch, sucrose, and galactose metabolism (7 metabolites). Overlap of significantly impacted pathways by RNA-Seq and metabolomics suggests amino acid breakdown and increased sugar import for energy production. Results indicate that LCO-exposed *Daphnia* are responding to energy starvation by altering metabolic pathways, both at the gene expression and metabolite level. These results support altered energy production as a sensitive nanotoxicity adverse outcome for LCO exposure and suggest negative impacts on energy metabolism as an important avenue for future studies of nanotoxicity, including for other biological systems and for metal oxide nanomaterials more broadly.

Introduction

In the field of nanotoxicology, the search for mechanisms of action has focused to a large extent on oxidative stress, with more than 7000 papers attributing toxicity of a diversity of engineered nanomaterials (ENMs) to this cause.[1–3] However, lost in the focus on reactive oxygen species (ROS) is research showing that ROS can be involved in numerous processes as signaling molecules,[4–6] as well as the importance of redox processes in cells for functions as universal as energy metabolism.[7] Importantly, for metal oxide ENMs, it has been demonstrated that overlap of the conduction band of these materials with the redox potential of biological reactions is predictive of toxicity.[8,9] In this way, redox active ENMs could interact with and impact critical biological processes that rely on redox chemistry, including metabolic pathways. However, the focus on ROS has prevented more sophisticated nanotoxicity mechanisms from being proposed, with oxidative stress suggested as the general cause of metal oxide ENM toxicity, in spite of clear metabolic impacts of these ENMs.[8,9]

Both the tricarboxylic acid (TCA) cycle, which produces reducing equivalents for the electron transport chain (ETC), and the ETC itself rely on redox processes to transfer electrons in order to produce large amounts of adenosine triphosphate (ATP) to meet cellular energy demands.[7,10,11] The centrality of redox processes in these widely conserved mechanisms of energy metabolism,[7] and the potential for metal oxide ENMs to interact with these processes,[8] indicate that these pathways could be an important target of metal oxide ENM toxicity, particularly at sublethal concentrations.

In fact, numerous studies have demonstrated metabolic impacts of metal oxide ENM exposures across cell and animal models. These include: a 5-fold increase in gluconeogenesis in rat liver cells exposed to ZnO ENM concentrations as low as 2.5 $\mu g/cm^2$, an effect not accountable by ion

dissolution alone;[12] significant negative impacts on primary production and respiration in algae exposed to nano-TiO_2 at 0.3 mg/L over 20 d;[13] a 4-fold decline in activity of tricarboxylic acid (TCA) cycle enzyme aconitase in 1 mg/L ZnO ENM-exposed white sucker liver;[14] reduced expression of 11 TCA cycle genes in CuO ENM-exposed *Pseudomonas aeruginosa* bacteria at 10 mg/L;[15] decreases in TCA cycle metabolites succinate, citrate, and α-ketoglutarate in kidney of ZnO-exposed rats at 100 mg/kg;[16] declines in TCA cycle metabolites citrate, fumarate, and malate by 4, 3, and 5-fold respectively in *C. elegans* exposed to nano-TiO_2 at 7.7 mg/L;[17] greater than 2-fold changes in expression of 115 electron transport chain (ETC) genes in human lung cells exposed to TiO_2 ENMs at 800 mg/L;[18] greater than 2-fold increased expression of ETC proteins ATP-synthase and ETF-α in mouse liver cells exposed to TiO_2 ENMs at 1 mg/L and ETC protein cytochrome b-c1 from exposure to ZnO and CuO ENMs at 5 mg/mL;[19] and 5-fold declines in NADH dehydrogenase activity and ATP production in mammalian cells exposed to Co_3O_4, Cr_2O_3, Ni_2O_3, CuO, Mn_2O_3, CoO, and ZnO ENMs at concentrations as low as 10 mg/L.[8] In spite of this evidence, the broad implication of the impact of a range of metal oxide ENMs on as universally-conserved of processes as energy metabolism has not been recognized. However, available evidence makes clear that the metabolic impacts of metal oxide ENMs should be concretely explored as a mechanism of nanotoxicity.

One class of transition metal oxide ENM that is relatively understudied in the nanotoxicology literature are the lithium intercalating cathode materials used in lithium ion batteries (LIBs): lithium cobalt oxide (LCO) and the alternative lithium nickel manganese cobalt oxide. The use of LIBs in electronic devices and increasingly in electric vehicles means an estimated 200,000 tons of these cathode materials were produced in 2020, and this is anticipated to rise to 380,000 tons annually by 2025, comparable to or exceeding production quantities of better-studied ENMs

such as Ag and TiO_2.[20–24] Less than 5% of these materials are currently recycled, with disposed material accumulating in landfills, where it may pose an environmental concern,[20,25,26] as some 16% of LIB cathode waste is leached from disposed material.[25] The 60,000 tons or more of LIB leachate annually that this represents puts it on par with TiO_2, a mass of material that could be of environmental concern.[20,27]

We have previously demonstrated that LCO is capable of negatively impacting survival and reproduction of the model aquatic invertebrate *Daphnia magna* at concentrations as low as 0.25 mg/L over 21 days.[28] *Daphnia magna* is a well-established and sensitive model for aquatic toxicology specifically, but with application as an important screening model for the toxicity of materials and compounds across species.[29] Previously, we showed that LCO causes negative impacts on growth, development, hemoglobin levels, expression of genes related to metabolism, and activity and oxidation state of the Fe-S TCA cycle enzyme aconitase in larvae of the sediment-dwelling midge *Chironomus riparius* at exposure concentrations as low as 10 mg/L.[27,30] It is our hypothesis that metabolic impacts of LCO will be observed across species due to the interaction of this ENM with conserved methods of energy metabolism. In order to determine if metabolic impacts of LCO are a mechanism conserved across species, and to gain further insight into potential metabolic changes resulting from LCO exposure, we employed RNA-Seq and metabolomics to examine global changes in gene expression and metabolite levels in response to a sublethal 1 mg/L LCO exposure in *D. magna* at 48 h.

Experimental Procedures

LCO nanosheet synthesis and characterization

The Li_xCoO_2 nanosheets used in this study were synthesized and characterized as previously described in Niemuth *et al*. 2020.[30] Detailed synthesis methods are included in the Supplementary information. Nanosheet surface area was determined by BET and found to be 125 m^2/g. Nanosheets were imaged edge-on using scanning electron microscopy and sheet-like structures were found to be consistent with previously published syntheses (Supplementary Figure S2).[31] Previously published transmission electron microscopy showed approximate nanosheet diameters of 25 nm and widths of 5 nm.[31] Powder X-Ray Diffraction patterns can be indexed to the $R\bar{3}m$ space group (Supplementary Figure S3), consistent with previously published work.[31] Nanosheet zeta potential was measured in moderately hard reconstituted water (MHRW) exposure media ($NaHCO_3$ 96 mg/L, $CaSO_4$ 60 mg/L, $MgSO_4$ 60 mg/L, KCl 4 mg/L, Na_2SeO_3 0.004 mg/L) with results of -12.6 ± 0.6 mV for 1 mg/L LCO (Zetasizer Nano ZS, Malvern), similar to previous results (Supplementary Table S1).[27] Supplementary Figure S4 shows quality data for zeta potential measurments.

RNA-Seq

Animal culture maintenance

Daphnia magna were obtained from Aquatic Research Organisms (Hampton, NH) and cultured following US EPA guidelines in moderately hard reconstituted water (MHRW; $NaHCO_3$ 96 mg/L, $CaSO_4$ 60 mg/L, $MgSO_4$ 60 mg/L, KCl 4 mg/L, Na_2SeO_3 0.004 mg/L in 18 MΩ ultrapure water), as in previous studies of LCO impacts in *Daphnia*.[28] Cultures were maintained at 20° C with a 16 h:8 h light:dark photoperiod, 20 adult daphnids per liter. Cultures were fed 3 times weekly with 25 mL *Raphidocelis subcapitata* (~500,000 algal cells/mL) and 10 mL alfalfa

solution (8 g *Medigo sativa* in 1 L of 18 MΩ ultrapure water). Media was changed 100% and neonates removed 3 times per week. Cultures were maintained using only third or fourth brood neonates less than 24 h old.

Exposure

Five replicates were prepared for each treatment: MHRW control, 1 mg/L LCO, and ion control (660 µg/L Li as LiCl and 150 µg/L Co as $CoCl_2$; 10× the ions released by 1 mg/L LCO in 48 h).[27] LCO exposure at 1 mg/L was chosen for this study as a concentration at which no negative impacts were apparent in daphnids at 48 h in our previous study, but which is known to cause impacts by 14 d.[28] This concentration also acts as a point of comparison to *C. riparius* larvae, which are unaffected by LCO at a 1 mg/L concentration.[27,30] Each replicate consisted of ten 5-day-old daphnids, which were then exposed for 48 h. Animals were fed alfalfa solution immediately after exposure setup and again after 24 h. After 48 h, animals were collected, pooled by replicate (*i.e.*, 5 replicates per condition, each replicate containing 10 pooled *Daphnia*), and flash frozen in liquid nitrogen. Flash frozen animals were then stored at -80ºC for subsequent RNA extraction, cDNA library creation, and next-generation RNA-Sequencing.

RNA-extraction, library preparation, and sequencing

Pooled flash frozen daphnids were homogenized by replicate in TRIzol (Thermo Fisher Scientific), and RNA was purified using the Direct-zol RNA MiniPrep kit (Zymo Research). RNA quality, determined using a NanoDrop 1000 spectrophotometer (Thermo Fisher Scientific), Bioanalyzer 2100 (Agilent), and Qubit fluorometer (Thermo Fisher Scientific), were: 260/280

ratio 1.8-2.0, 260/230 ratio 2.0-2.2, and RIN > 7. RNA sequencing libraries were prepared from 200 ng of total RNA from each sample using the Illumina TruSeq Stranded mRNA kit (Illumina, RS-122-2102) and IDT for Illumina – TruSeq RNA UD Indexes (Illumina, 20022371). Prepared libraries were then sequenced using an Illumina NovaSeq6000, with paired-end reads of 150 bp. Data are available from the NCBI Gene Expression Omnibus (GEO) under accession number GSE174016.

Processing of RNA-Seq data

Raw sequence data from the Illumina NovaSeq 6000 instrument gave a total genomic yield surpassing 919 million paired-end reads, a median per-sample yield of 41.85 million fragments, and a population standard deviation of 9.811 million fragments. FastQC v0.11.5 was used to quality assess the sequence data,[32] and no apparent base-calling errors needed to be removed. Illumina TruSeq 3'-anchored primers were clipped using Cutadapt v1.18,[33] and the resulting quality-controlled data was pseudoaligned and sample-quantified against the daphmag2.4 Ensembl release of the *Daphnia magna* reference transcriptome using Kallisto v0.45.0.[34] Differential expression analysis of sample pairs was performed using the DESeq2 package[35] within R v3.5.3, and the resulting tables of differentially expressed transcripts were re-annotated with Ensembl reference information and relationally joined with Kallisto sample quantification counts using custom tooling. As limited annotation data exists for *D. magna* genes, assembled contigs were annotated against the Refseq protein database for the well-annotated model invertebrate *Drosophila melanogaster* (e-value ≤ 0.1) using the BLASTX tool in the NCBI-BLAST+ package v2.2.28.[36] High-throughput parallelization of Kallisto was achieved using a

high-performance computer cluster leveraging the Slurm job scheduler,[37] while all other steps were completed using a high-performance local workstation employing GNU Parallel.[38]

RNA-Seq data analysis using DAVID and KEGG

A total of 17,604 contigs were successfully assembled and present in at least 80% of samples. Of these, 15,223 were successfully annotated against *D. melanogaster* using BLASTX. 3,280 contigs were differentially expressed between MHRW control and 1 mg/L LCO samples (Wald FDR < 0.1) and found in at least 80% of samples. Of these, 2,988 could be annotated against *D. melanogaster*. These differentially expressed, annotated contigs were analyzed for functional enrichment using the Database for Annotation, Visualization and Integrated Discovery (DAVID) using a Benjamini-adjusted FDR < 0.1.[39,40] Pathway analysis was performed using the Kyoto Encyclopedia of Genes and Genomes (KEGG) mapper based on assigned KEGG orthology (KO) terms.[41–43] Of annotated, differentially expressed contigs between MHRW control and 1 mg/L LCO samples, 2,446 could be assigned functions in DAVID and 1,071 could be assigned KOs by KEGG.

Metabolomics

Daphnid cultures

D. magna were cultured as indicated above: density of 20 animals per liter MHRW, 16 h:8 h light:dark photoperiod, and a temperature of 20 °C. For metabolomics, cultures were fed daily on suspensions of unicellular green alga, *Chlorella vulgaris* (7.84×10^7 cells/mL) at 2 mL/L. Algae

was supplemented daily by 50 µL/L of dried bakers yeast (1mg/mL stock, Sigma–Aldrich) to conform to protocols previously established for metabolomics analysis in *Daphnia magna*.[44] Cultures were maintained using third or fourth brood neonates less than 24 h old.

Exposure Details and Procedures

Ten replicates were prepared for each treatment: MHRW control, 1 mg/L LCO, and ion control (66 µg/L Li as LiCl and 15 µg/L Co as $CoCl_2$; equivalent to ions released by 1 mg/L LCO over 48 h).[27,28] Twenty neonates per replicate (< 9 h old) were transferred to 100 ml beakers 48 hours prior to exposure and fed proportionate amounts of food for 48 hours. At the end of the 48-hour feeding period, daphnids were transferred to 200 ml control or exposure beakers. Exposures were carried out for 48 h without food per standard OECD guidelines for *D. magna*.

At the end of the exposure daphnids were collected and transferred (20 pooled animals per replicate) into labeled Precellys tubes using a fine sable brush and flash frozen in liquid nitrogen. Samples were stored at -80 °C and shipped to the University of Birmingham, UK on dry ice.

Daphnia Tissue Extraction

For the extraction, all solvents were chilled to 4 ºC. A mixture of 320 µL of HPLC grade MeOH and 128 µL of HPLC grade H_2O were added to each sample tube and kept on ice. Tubes were then placed in a Precellys 24 homogeniser for 2 × 10s bursts at 6400 rpm. The homogenised mixture was then transferred into a clean 1.8 mL glass vial (Fisher TUL 520 006 J) using a

Pasteur pipette. 320 µL (32 µL/mg) $CHCl_3$ (HPLC grade) and 160 µL (16 µL/mg) dH_2O (HPLC grade) were then added to each vial. These vials were vortexed on full power for 15 s each to thoroughly mix polar and non-polar solvents. Vials were then left on ice for on ice for 10 min to allow initial phase separation. Vials were then centrifuged at 4000 rpm at 4 ºC for 10 min to ensure complete phase separation. Centrifuged vials were allowed to come to room temperature by setting them on the lab bench for 5 min.

Samples were then visibly biphasic, with protein debris separating the upper (polar) and lower (non-polar) layers. A 500 uL Hamilton syringe was then used to remove the polar phase (~ 2 × 150 µL aliquots) into 2 clean 1.5 mL Eppendorf tubes (one for positive, one for negative ion analysis). Polar samples were then dried using a Speed Vac concentrator and stored at -80 °C until analysis.

Sample Preparation and Direct Infusion Mass Spectrometry Metabolomics

For positive ion analysis, 30 µL of 4 ºC 80:20 methanol:water plus 0.25% formic acid was added to each of the frozen, dried extracts, and each sample vortexed for 30s. For negative ion analysis 30 µL of 4 ºC 80:20 methanol:water plus 20 mM ammonium acetate was added to each of the frozen, dried extracts, and each sample vortexed for 30 s. Samples were then centrifuged at 4000 g at 4 ºC for 10 mins. For both positive and negative ion analyses, samples were randomized and 5 µL of sample supernatant was pipetted into a pre-washed 96-well sample plate in quadruplicate. Three quality control (QC) samples (a mixture with equal volume from all samples) and a blank were also included on each plate. Loaded plates were covered with a foil

seal using heat sealer and loaded into a TriVersa Nano-Mate® nanoelectro-spray ion source (Advion) with the cooler set at 10 ºC. Non-targeted analysis was carried out on polar fractions by direct infusion mass spectrometry (DIMS) using an LTQ Orbitrap Elite (Thermo Fisher Scientific). Twenty-one overlapping selected ion monitoring (SIM) windows were collected covering m/z values from 50 to 620. Data are available in the NIH National Metabolomics Data Repository (NMDR) under project number PR001141.

Data analysis

The Galaxy pipeline at the University of Birmingham[45] was used to process raw data collected. SIM windows were assembled into single spectra for each sample (SIM-Stitching).

A signal to noise ratio (SNR) of 10 was selected to filter out background noise from the data. A replicate filter was applied to retain only peaks found in at least 3 out of 4 technical replicates, and samples aligned across biological samples. A blank filter was applied to only retain peaks if they are a specified % larger than blank values. Finally a sample filter was applied to keep only those peaks found in greater than 80% of biological samples.

Probabilistic quotient normalization (PQN) was applied to normalize the DIMS metabolomics data to account for differences in dilution between samples. A K-nearest neighbor (KNN) algorithm was then applied to impute missing values. A generalized-log transformation was then applied to stabilize the technical variance of the DIMS measurements. To assess data quality, the

median relative standard deviation (RSD) was measured across technical replicates and an RSD cutoff value of 10 was specified.

Univariate ANOVAs were carried out on metabolite data with a false discovery rate (FDR) correction to account for the large number of possible comparisons. Peaks were annotated using the Functional Analysis tool for MS peaks on the MetaboAnalyst 5.0 online web server.[46] Peak list files were uploaded containing m/z values and FDR corrected p-values obtained by the processing above, and analyzed in the respective (positive or negative) ion mode with a 5.0 ppm mass tolerance. For enrichment analysis, the Mummichog algorithm was applied with a p-value cutoff of $p < 0.1$ and analyzed against the KEGG database for *Homo sapiens* and *Drosophila melanogaster*.

Results and Discussion

RNA-Seq supports metabolic response to LCO exposure

DAVID enrichment analysis shows significant enrichment (Benjamini-adjusted $p < 0.1$) for a series of gene ontology (GO) terms, UniProt keywords, and KEGG pathways associated with energy metabolism for genes identified by RNA-Seq as differentially expressed (Wald FDR-adjusted $p < 0.01$) between MHRW control and 1 mg/L LCO-exposed *D. magna* at 48 h (Table 1). Specifically, 8 different categories related to components and functioning of the electron transport chain (ETC) are significantly enriched: Mitochondrial respiratory chain complex I, 17 genes, $p = 0.0002$; Ubiquinone, 16 genes, $p = 0.0004$; Oxidoreductase, 80 genes, $p = 0.0006$; Mitochondrion, 70 genes, $p = 0.004$; Oxidative phosphorylation, 53 genes, $p = 0.01$; NADH

dehydrogenase activity, 12 genes, p = 0.05; NADH dehydrogenase (ubiquinone) activity, 13 genes, p = 0.05; and Mitochondrial electron transport, NADH to ubiquinone, 12 genes, p = 0.06. The cellular response to energy starvation was also specifically identified as enriched by DAVID (25 genes, p = 0.002), as well as ATP binding (70 genes, p = 0.006) and one-carbon metabolism (5 genes, p = 0.07).

The electron transport chain is the primary energy source for all multicellular eukaryotes, utilizing reducing equivalents such as NADH derived from the breakdown of sugars, amino acids, and fatty acids in the tricarboxylic acid (TCA) cycle to produce adenosine triphosphate (ATP), the so-called "energy currency of the cell," essential for life due to its use as the energy source for numerous biochemical processes.[10,11] Figure 1 demonstrates the specific genes in the ETC differentially expressed (Wald FDR-adjusted $p < 0.01$) in *D. magna* exposed to LCO at 1 mg/L for 48 h versus control animals. As can be seen (Fig 1, Supplementary Table S2), 34 different ETC genes are upregulated in response to LCO exposure, including 20 components of Complex I (NADH dehydrogenase Fe-S proteins *NDUFS2*, *3*, *4*, *6*, and *8*; NADH dehydrogenase flavoprotein 1 *NDUFV1*; NADH dehydrogenase 1 alpha subcomplex subunits *NDUFA2*, *4*, *5*, *6*, *7*, *10*, *12*, and *13*; and NADH dehydrogenase 1 beta subunits *NDUFB2*, *3*, *4*, *9*, *10*, and *11*; note that NADH dehydrogenase activity and NADH dehydrogenase ubiquinone activity were identified as significantly enriched by DAVID, Table 1), one subunit of Complex II (succinate dehydrogenase flavoprotein subunit *SDHA*), two components of Complex III (ubiquinol-cytochrome c reductase subunits *QCR7* and *QCR8*), five components of Complex IV (cytochrome c oxidase subunits *COX 1*, *4*, *5B*, *6A*, and *6B*), and six components of Complex V (F-type H^+-transporting ATPase subunits *ATPeF0B*, *D*, *F*, *F6*, and *O*, and F-type H^+-transporting ATPase subunit epsilon *ATPeF1E*).

Complex I, also known as NADH dehydrogenase, is the critical first complex of the ETC and allows the transfer of electrons from NADH into the ETC, transferring electrons via an FMN cofactor, through a series of Fe-S centers, and ultimately to ubiquinone, pumping protons into the mitochondrial intermembrane space in the process.[47] We previously showed that expression of Complex I subunit genes as well as levels of Complex I Fe-S centers are upregulated in response to LCO exposure in larvae of sediment-dwelling invertebrate *Chironomus riparius*.[30] NADH dehydrogenase activity has also been shown to be negatively impacted by metal oxide ENM exposure in mammalian cells.[8] Thus, changes in Complex I may be a sensitive indicator of metal oxide ENM toxicity across species and particle types.

Complex II, Succinate dehydrogenase, is also an Fe-S enzyme complex, and uses an FAD cofactor to transfer electrons from succinate through a series of Fe-S centers to ubiquinone. Like Complex I, succinate dehydrogenase genes and Fe-S centers are also increased in response to LCO exposure in *C. riparius*.[30] Complexes III and IV, Cytochrome c reductase and Cytochrome c oxidase, are involved in transferring electrons to Cytochrome c from ubiquinol and from cytochrome c to oxygen, respectively.[10] Cytochrome c itself was shown to be oxidized by metal oxide ENMs (including CoO and Co_2O_3) *in vitro*,[8] which may indicate that metal oxide ENMs are capable of interacting directly with redox-active cellular components, including in the ETC. Complex V, ATP synthase, utilizes the proton gradient created by electron transfer in Complexes I, III, and IV, to couple P_i and ADP, creating ATP.[10] ATP production was shown to be negatively impacted in mammalian cells exposed to metal oxide ENMs,[8] indicating that the ultimate endpoint of oxidative metabolism can indeed be negatively impacted by metal oxide ENM exposure.

In this study, the upregulation of these ETC components (Fig 1), along with enrichment of genes associated with energy starvation (Table 1), clearly demonstrate the negative impacts of LCO on metabolism, and also provide evidence that may explain the impacts of LCO and other complex metal oxide ENMs on the growth and reproduction of *D. magna* after exposure to these materials in the literature,[28] as well as growth and development impacts observed for the sediment-dwelling invertebrate *Chironomus riparius*.[27] These results also accord well with previous demonstrations of metabolic impacts of LCO in other models by RNA-Seq, both in *C. riparius* larvae and in gill cell culture from trout species *Oncorhynchus mykiss*, where metabolism was identified as significantly enriched.[30,48] Impacts of other metal oxides on expression of genes in the ETC have also been demonstrated for TiO_2 nanoparticles,[18] and exposure to numerous metal oxide nanoparticles (i.e. Co_3O_4, Cr_2O_3, Ni_2O_3, CuO, Mn_2O_3, CoO, ZnO) have been demonstrated to negatively impact metabolism of cells *in vitro*, specifically by reducing NADH dehydrogenase activity as measured by MTS assay as well as ATP production at sub-cytotoxic concentrations.[8] Thus, metabolism may be a sensitive endpoint for metal oxide ENM exposure, showing impacts at sub-lethal exposure concentrations in *Daphnia* in this study, as well as for chironomids,[30] trout gill cells,[48] and mammalian cell culture.[8,18]

Also supporting impacts related to the ETC, and specifically to ATP, is the identification by DAVID of enrichment for Plasma membrane proton-transporting V-type ATPase complex (13 genes; Benjamini-adjusted p = 0.002) and ATP hydrolysis coupled proton transport (18 genes; Benjamini-adjusted p = 0.06). As shown in Fig 1, 13 subunits of the vacuole-localized V-type H^+-transporting ATPase (*ATPeV0A, 0B, 0C, 0D, 0E, 1A, 1B, 1C, 1D, 1E, 1F, 1G,* and *1H*) are all downregulated. This transporter uses ATP to pump protons into vacuoles,[49] and its downregulation suggests conservation of ATP as a result of energy starvation.

Downregulated components of the ETC include Complex IV genes heme a synthase (*COX15*) and cytochrome c oxidase assembly subunit 17 (*COX17*), both potentially related to metal homeostasis (Fig 1). *COX15* is involved in synthesizing the heme a cofactor for Complex IV.[50] Heme synthesis was also seen as being downregulated by LCO exposure in *C. riparius* larvae,[27] and heme-containing catalase was downregulated in *D. magna* as a result of LCO exposure by qPCR.[28] We proposed that the heme impacts of LCO exposure were the result of deregulation of iron homeostasis as a result of oxidation of the Fe-S center of the iron-responsive protein, which we showed to be oxidized using both activity assay and electron paramagnetic resonance in *C. riparius* larvae.[30] *COX17* is involved in the transfer of copper during the assembly of Complex IV.[51] It's downregulation could indicate a broader disruption of metal homeostasis as a result of LCO exposure. Disruption of iron homeostasis was indicated by RNA-Seq in *C. riparius* larvae exposed to LCO.[30]

Also identified as enriched by DAVID (Benjamini-adjusted $p < 0.1$) were a series of terms related to protein synthesis, degradation, and amino acids (Table 1). Specifically enriched were: Ribosome biogenesis, 21 genes, $p = 0.0009$; Protein biosynthesis, 40 genes, $p = 0.003$; Aminoacyl-tRNA synthetase, 20 genes, $p = 0.003$; Ribosome biogenesis in eukaryotes, 38 genes, $p = 0.01$; Protein export, 17 genes, $p = 0.01$; Protease, 86 genes, $p = 0.02$; Aminoacyl-tRNA biosynthesis, 25 genes, $p = 0.08$; and rRNA processing, 13 genes, $p = 0.08$. Supplementary Table 1 shows that genes in KEGG pathways for Ribosome biogenesis (37 genes), Ribosome (30 genes), Protein export (16 genes), and Aminoacyl-tRNA biosynthesis (26 genes) are all downregulated. These processes are all necessary for protein synthesis, and their coordinated downregulation suggests a metabolic shift away from anabolic processes like protein synthesis and, as will be discussed in the context of metabolomics data below, toward catabolism,

specifically the breakdown of proteins for energy. The enrichment for protease genes (Table 1), necessary for the breakdown of proteins into amino acids, also supports this conclusion.

Metabolomics and RNA-Seq support metabolic switch to energy production

Table 2 shows enriched KEGG pathways as identified by MetaboAnalyst (gamma-adjusted $p < 0.1$) for metabolites significantly different (FDR-adjusted $p < 0.1$) between MHRW control and 1 mg/L LCO exposed daphnids at 48 h. As can be seen, amino acid metabolism is the most common pathway type identified as significantly enriched among putatively annotated metabolites, with 10 enriched pathways: Histidine metabolism, 3 metabolites, $p = 0.02$; beta-Alanine metabolism, 4 metabolites, $p = 0.03$; Valine leucine and isoleucine biosynthesis, 3 metabolites, $p = 0.03$; Aminoacyl-tRNA biosynthesis, 5 metabolites, $p = 0.04$; D-Arginine and D-ornithine metabolism, 2 metabolites, $p = 0.05$; Tryptophan metabolism, 3 metabolites, $p = 0.05$; Valine leucine and isoleucine degradation, 3 metabolites, $p = 0.07$; Glycine serine and threonine metabolism, 3 metabolites, $p = 0.08$; Lysine degradation, 2 metabolites, $p = 0.08$; and Arginine and proline metabolism, 3 metabolites, $p = 0.09$.

The combination of metabolomics results with RNA-Seq data for differentially expressed genes demonstrates important overlap between significantly changed amino acid metabolites, their breakdown metabolite intermediates, and expression changes for genes of enzymes involved in amino acid metabolism and degradation between MHRW control and 1 mg/L LCO-exposed daphnids (Supplementary Table S2). Particularly striking are the lower levels of the amino acids L-Leucine (Leu), L-Valine (Val), and L-Isoleucine (Ile), the increased levels of their breakdown intermediates Isoveryl-CoA and (S)-2-Methylbutanoyl-CoA, and the increase in expression of 14

genes for enzymes involved in the breakdown of these amino acids (Fig 2). These changes support the breakdown of these amino acids to produce Acetyl-CoA, the critical entry metabolite for production of reducing equivalents in the TCA cycle (and ultimately ATP in the ETC).[11] Other changes observed in combined metabolomics and RNA-Seq data supporting this conclusion are changes in Tryptophan metabolism, specifically the increase in levels of 7 putatively annotated breakdown intermediates for Tryptophan (L-Kynurenine, 5-Hydroxy-L-tryptophan, 3-Hydroxy-L-kynurenine, Formyl-5-hydroxykynurenamine, 5-Hydroxy-N-formylkynurenine, 5-Hydroxykynurenine, N-Methyltryptamine) and increased expression for 6 enzyme genes involved in Tryptophan degradation (glutaryl-CoA dehydrogenase, tryptophan 5-monooxygenase, dihydrolipoamide succinyltransferase, arylalkylamine N-acetyltransferase, L-tryptophan decarboxylase, and enoyl-CoA hydratase; Supplementary table S2). As was noted above, 26 genes involved in Aminoacyl-tRNA biosynthesis, that is loading of amino acids onto tRNAs for subsequent protein synthesis, are all downregulated (Supplementary Table S2). The amino acids to be loaded in this process that are lower in LCO-exposed animals are: L-Arginine, L-Leucine, L-Histidine, L-Valine, and L-Isoleucine (Supplementary Table S2). Taken together, decreases in protein synthesis genes, enrichment for protease genes, decreases in levels of amino acids, increases in amino acid breakdown intermediates, and increases in expression of enzyme genes involved in breakdown of amino acids support a shift in LCO-exposed animals toward protein catabolism, likely in response to energy starvation (seen as enriched by DAVID, Table 1).

Also found to be enriched by MetaboAnalyst are Starch and sucrose metabolism (4 putatively annotated metabolites, gamma-adjusted $p = 0.03$) and Galactose metabolism (6 putatively annotated metabolites, gamma-adjusted $p = 0.04$; Table 2). Unlike amino acids, similarities in

mass between sugar isomers and other transformation products makes positive identification of specific sugars difficult by DIMS. However, as seen in Table 3, ions putatively corresponding to 7 sugars are all increased in LCO-exposed daphnids. Corresponding changes in expression of Starch and sucrose metabolism and Galactose metabolism can also be seen by RNA-Seq (Supplementary Table S2). Increases in expression of glucose transporters was previously seen in trout gill cells exposed to LCO.[48] The increase in sugars in LCO-exposed daphnids, like the breakdown of amino acids, supports a response in exposed animals to energy starvation.

Taken together, changes observed by both RNA-Seq and metabolomics support metabolic changes in *Daphnia* in response to LCO exposure toward increasing energy production, likely as a response to energy starvation. These include: enrichment of gene expression changes related to the Cellular response to energy starvation and to Oxidative phosphorylation (Table 1), the upregulation of ETC components and downregulation of ATP using complexes (Fig 1), the enrichment for and downregulation of genes involved in protein synthesis (Table 1; Supplementary Table S2), decreases in levels of amino acids and increases in their breakdown products and expression of amino acid degradation enzyme genes (Table 2, Fig 2, Supplementary Table S2), and increases in levels of sugars (Table 3) and changes in sugar metabolism enzyme genes (Supplementary Table S2). These results accord with metabolic impacts seen from LCO and other metal oxides in the literature including changes in metabolic gene expression in *C. riparius* larvae and trout gill cells exposed to LCO,[30,48] changes in expression of oxidative phosphorylation genes in human lung cells following TiO_2 exposure,[18] reduced in NADH dehydrogenase activity and ATP production in mammalian cells exposed to a range of metal oxide ENMs,[8] and metabolic changes observed in components of the TCA cycle and ETC from exposure to numerous metal oxide ENMS in different biological systems.[14–17,19]

Metal oxide ENMs have also been shown to impact function of mitochondria in both yeast and plants, as well as function of plant chloroplasts.[52] Thus, evidence both provided by this study as well as that available in the literature suggest that metabolic impacts of metal oxide ENMs may be a mechanism of nanotoxicity applicable across species and particle type.

Released ion control showed no significant impact on metabolites versus MHRW control at concentrations equivalent to that released by 1 mg/L LCO at 48 h (66 μg/L Li and 15 μg/L Co). RNA-Seq showed gene-expression changes for ion exposure only at a concentration equivalent to 10× the ions released from 1 mg/L LCO in 48 h (660 μg/L Li and 150 μg/L Co).[27] In this case, DAVID functional enrichment terms shared with particles included the Ribosome KEGG pathway (Benjamini-adjusted $p = 0.000002$) but did not include enrichment for oxidative phosphorylation or other ETC components, demonstrating the nano-specificity of metabolic impacts of LCO.

Potential mechanism and implications of metabolic impacts

The mechanism by which LCO and other metal oxide ENMs may be able to impact metabolism has been suggested in the literature, but only from the standpoint of ROS generation and oxidative stress, ultimately missing what may be a far more nuanced process with broad implications: the ability of metal oxide ENMs to participate in redox chemistry.[8,20] Zhang *et al*. 2012 demonstrate that the overlap of the conduction band of metal oxide ENMs with the biological redox potential is predictive of toxicity, including reduced NADH dehydrogenase activity and ATP production.[8] In the case of LCO, its bandgap energy is similar to that of CO_3O_4 nanoparticles shown to negatively impact metabolism in Zhang *et al*. 2012 (2.7 versus 2.53 eV

respectively),[8,53,54] supporting the possibility that LCO's bandgap may explain its metabolic impacts in this and other studies.[30,48] Zhang *et al*. 2012 also show oxidation of cytochrome c by these metal oxide ENMs, but ultimately attribute impacts to general oxidative stress.[8] Hamers 2020 proposes that the toxicity of LCO may be due to reduction of Co^{3+} to Co^{2+} during metal release into aqueous solution, with concomitant oxidation of other species to produce ROS.[20] LCO has been shown to oxidize the non-specific ROS-sensitive fluorescent dye CM-H_2DCFDA in trout gill cells[55] and oxidize the Fe-S center of aconitase in *C. riparius* lavae,[30] indicating that it can participate directly or indirectly in redox processes. An important point in this context is that energy metabolism is reliant on redox processes[7] and may thus represent a sensitive endpoint to redox-active materials, potentially as a result of redox chemistry occurring at the particle surface or via an ROS intermediate. This could be the result of the overlap of the redox potential of these metabolic processes with the ENM conduction band, of oxidative metal release, or of the combination of these or other redox processes. The conservation of these redox-dependent processes for energy metabolism across eukaryotes,[7,10] and the conservation of energy metabolism across species more broadly,[56] in combination with the observation of changes in energy metabolism in response to metal oxide ENM exposure across metal types and biological systems,[8,12–19,30,48] suggest that this may be a fruitful avenue of future nanotoxicity research, both from the standpoint of chemistry and biology.

The time course and reversibility of these impacts also remain to be studied, as well as systematic validation of the conservation of cross-species impacts of metal oxide ENMs on energy metabolism, determination of species-specific impacts or strategies for mitigating these impacts (*e.g*. anaerobic metabolism in bacteria and yeast), exploration of impacts on conserved

molecular targets (*e.g.* Fe-S centers, as identified in *C. riparius*)[30] across species, and the effect of impacts on energy metabolism on reproduction, fitness of offspring, and the food web.

Conclusion

We have provided evidence that metal oxide ENM LCO impacts energy metabolism in the model invertebrate *Daphnia magna* at both the gene expression and metabolite level, and proposed the reactivity of metal oxide ENMs with redox-dependent biological processes as a likely mechanism for these impacts. This study contributes to a growing body of evidence that metal oxide ENMs negatively impact energy metabolism across species, from bacteria[9] to yeast, plants,[52] invertebrates,[30] and mammalian cells.[8] By providing evidence for specific pathways impacted using both gene expression and metabolomic techniques, namely components of the ETC and pathways involved in energy metabolism (Table 1, Fig 1) and impacted metabolites related to energy metabolism (Table 2, Fig 2, Table 3), this study provides important molecular targets for future investigation both across species and ENM types. The techniques employed also point the way for potentially fruitful studies of the metabolic impact of metal oxide ENMs across species, and the proposed mechanism, in the context of the literature, points to likely conservation of these impacts across metal oxide ENMs.

Acknowledgement

This material is based upon work supported by the National Science Foundation under Grant No. CHE-2001611, the NSF Center for Sustainable Nanotechnology. The CSN is part of the Centers for Chemical Innovation Program. This project used the UW-Milwaukee Great Lakes Genomics Center for RNA isolation, Illumina NovaSeq RNA sequencing, and bioinformatics services.

Metabolomics experiments were carried out in the Environmental Metabolomics Research Laboratory at the University of Birmingham.

Conflict of interest statement

The authors have no conflicts to declare.

Supporting Information

Supplementary information. PDF including supplementary figures and tables referenced in the text.

References

(1) Murphy, C. J.; Vartanian, A. M.; Geiger, F. M.; Hamers, R. J.; Pedersen, J.; Cui, Q.; Haynes, C. L.; Carlson, E. E.; Hernandez, R.; Klaper, R. D.; Orr, G.; Rosenzweig, Z. Biological Responses to Engineered Nanomaterials: Needs for the Next Decade. *ACS Cent. Sci.* **2015**, *1* (3), 117–123. https://doi.org/10.1021/acscentsci.5b00182.

(2) Chen, X. Mapping the Decadal (2009–2018) Research Landscape of Nanotoxicity: Insights from a Bibliometric Study. *Nanosci. Nanotechnol. Lett.* **2019**, *11* (10), 1327–1337. https://doi.org/10.1166/nnl.2019.3015.

(3) Abbas, Q.; Yousaf, B.; Ullah, H.; Ali, M. U.; Ok, Y. S.; Rinklebe, J. Environmental Transformation and Nano-Toxicity of Engineered Nano-Particles (ENPs) in Aquatic and

Terrestrial Organisms. *Crit. Rev. Environ. Sci. Technol.* **2020**, *50* (23), 2523–2581. https://doi.org/10.1080/10643389.2019.1705721.

(4) Ray, P. D.; Huang, B.-W.; Tsuji, Y. Reactive Oxygen Species (ROS) Homeostasis and Redox Regulation in Cellular Signaling. *Cell. Signal.* **2012**, *24* (5), 981–990. https://doi.org/10.1016/J.CELLSIG.2012.01.008.

(5) Choudhary, A.; Kumar, A.; Kaur, N. ROS and Oxidative Burst: Roots in Plant Development. *Plant Divers.* **2020**, *42* (1), 33–43. https://doi.org/10.1016/j.pld.2019.10.002.

(6) Devireddy, A. R.; Zandalinas, S. I.; Fichman, Y.; Mittler, R. Integration of Reactive Oxygen Species and Hormone Signaling during Abiotic Stress. *Plant J.* **2021**, *105* (2), 459–476. https://doi.org/10.1111/tpj.15010.

(7) Griffiths, H. R.; Gao, D.; Pararasa, C. Redox Regulation in Metabolic Programming and Inflammation. *Redox Biol.* **2017**, *12*, 50–57. https://doi.org/10.1016/j.redox.2017.01.023.

(8) Zhang, H.; Ji, Z.; Xia, T.; Meng, H.; Low-Kam, C.; Liu, R.; Pokhrel, S.; Lin, S.; Wang, X.; Liao, Y.-P.; Wang, M.; Li, L.; Rallo, R.; Damoiseaux, R.; Telesca, D.; Mädler, L.; Cohen, Y.; Zink, J. I.; Nel, A. E. Use of Metal Oxide Nanoparticle Band Gap To Develop a Predictive Paradigm for Oxidative Stress and Acute Pulmonary Inflammation. *ACS Nano* **2012**, *6* (5), 4349–4368. https://doi.org/10.1021/nn3010087.

(9) Kaweeteerawat, C.; Ivask, A.; Liu, R.; Zhang, H.; Chang, C. H.; Low-Kam, C.; Fischer, H.; Ji, Z.; Pokhrel, S.; Cohen, Y.; Telesca, D.; Zink, J.; Mädler, L.; Holden, P. A.; Nel, A.; Godwin, H. Toxicity of Metal Oxide Nanoparticles in *Escherichia coli* Correlates with Conduction Band and Hydration Energies. *Environ. Sci. Technol.* **2015**, *49* (2), 1105–

1112. https://doi.org/10.1021/es504259s.

(10) Chaban, Y.; Boekema, E. J.; Dudkina, N. V. Structures of Mitochondrial Oxidative Phosphorylation Supercomplexes and Mechanisms for Their Stabilisation. *Biochim. Biophys. Acta - Bioenerg.* **2014**, *1837* (4), 418–426. https://doi.org/10.1016/j.bbabio.2013.10.004.

(11) Polyzos, A. A.; McMurray, C. T. The Chicken or the Egg: Mitochondrial Dysfunction as a Cause or Consequence of Toxicity in Huntington's Disease. *Mech. Ageing Dev.* **2017**, *161*, 181–197. https://doi.org/10.1016/j.mad.2016.09.003.

(12) Filippi, C.; Pryde, A.; Cowan, P.; Lee, T.; Hayes, P.; Donaldson, K.; Plevris, J.; Stone, V. Toxicology of ZnO and TiO_2 Nanoparticles on Hepatocytes: Impact on Metabolism and Bioenergetics. *Nanotoxicology* **2015**, *9* (1), 126–134. https://doi.org/10.3109/17435390.2014.895437.

(13) Cardinale, B. J.; Bier, R.; Kwan, C. Effects of TiO_2 Nanoparticles on the Growth and Metabolism of Three Species of Freshwater Algae. *J. Nanoparticle Res.* **2012**, *14* (8), 913. https://doi.org/10.1007/s11051-012-0913-6.

(14) Dieni, C. A.; Callaghan, N. I.; Gormley, P. T.; Butler, K. M. A.; MacCormack, T. J. Physiological Hepatic Response to Zinc Oxide Nanoparticle Exposure in the White Sucker, *Catostomus commersonii*. *Comp. Biochem. Physiol. Part C Toxicol. Pharmacol.* **2014**, *162*, 51–61. https://doi.org/10.1016/j.cbpc.2014.03.009.

(15) Guo, J.; Gao, S.-H.; Lu, J.; Bond, P. L.; Verstraete, W.; Yuan, Z. Copper Oxide Nanoparticles Induce Lysogenic Bacteriophage and Metal-Resistance Genes in *Pseudomonas aeruginosa* PAO1. *ACS Appl. Mater. Interfaces* **2017**, *9* (27), 22298–22307.

https://doi.org/10.1021/acsami.7b06433.

(16) Yan, G.; Huang, Y.; Bu, Q.; Lv, L.; Deng, P.; Zhou, J.; Wang, Y.; Yang, Y.; Liu, Q.; Cen, X.; Zhao, Y. Zinc Oxide Nanoparticles Cause Nephrotoxicity and Kidney Metabolism Alterations in Rats. *J. Environ. Sci. Heal. Part A* **2012**, *47* (4), 577–588. https://doi.org/10.1080/10934529.2012.650576.

(17) Ratnasekhar, C.; Sonane, M.; Satish, A.; Mudiam, M. K. R. Metabolomics Reveals the Perturbations in the Metabolome of *Caenorhabditis elegans* Exposed to Titanium Dioxide Nanoparticles. *Nanotoxicology* **2015**, *9* (8), 994–1004. https://doi.org/10.3109/17435390.2014.993345.

(18) Jayaram, D. T.; Kumar, A.; Kippner, L. E.; Ho, P.-Y.; Kemp, M. L.; Fan, Y.; Payne, C. K. TiO_2 Nanoparticles Generate Superoxide and Alter Gene Expression in Human Lung Cells. *RSC Adv.* **2019**, *9* (43), 25039–25047. https://doi.org/10.1039/C9RA04037D.

(19) Tedesco, S.; Bayat, N.; Danielsson, G.; Buque, X.; Aspichueta, P.; Fresnedo, O.; Cristobal, S. Proteomic and Lipidomic Analysis of Primary Mouse Hepatocytes Exposed to Metal and Metal Oxide Nanoparticles. *J. Integr. OMICS* **2015**, *5* (1). https://doi.org/10.5584/jiomics.v5i1.184.

(20) Hamers, R. J. Energy Storage Materials as Emerging Nano-Contaminants. *Chem. Res. Toxicol.* **2020**, acs.chemrestox.0c00080. https://doi.org/10.1021/acs.chemrestox.0c00080.

(21) Brodd, R. J. Batteries for Sustainability *: Selected Entries from the Encyclopedia of Sustainability Science and Technology*; Springer, 2012.

(22) Grey, C. P.; Ceder, G.; Kang, K.; Meng, Y. S.; Bre, J. Electrodes with High Power and

High Capacity for Rechargeable Lithium Batteries. *Science (80-.).* **2005**, *311* (December), 1–5. https://doi.org/10.1126/science.1122152.

(23) Pollet, B. G.; Staffell, I.; Shang, J. L. Current Status of Hybrid, Battery and Fuel Cell Electric Vehicles: From Electrochemistry to Market Prospects. *Electrochim. Acta* **2012**, *84*, 235–249. https://doi.org/10.1016/j.electacta.2012.03.172.

(24) Wang, Y.; Yu, Y.; Huang, K.; Chen, B.; Deng, W.; Yao, Y. Quantifying the Environmental Impact of a Li-Rich High-Capacity Cathode Material in Electric Vehicles via Life Cycle Assessment. *Environ. Sci. Pollut. Res.* **2017**, *24* (2), 1251–1260. https://doi.org/10.1007/s11356-016-7849-9.

(25) Winslow, K. M.; Laux, S. J.; Townsend, T. G. A Review on the Growing Concern and Potential Management Strategies of Waste Lithium-Ion Batteries. *Resources, Conservation and Recycling*. Elsevier 2018, pp 263–277. https://doi.org/10.1016/j.resconrec.2017.11.001.

(26) Hamers, R. J. Nanomaterials and Global Sustainability. *Acc. Chem. Res.* **2017**, *50* (3), 633–637. https://doi.org/10.1021/acs.accounts.6b00634.

(27) Niemuth, N. J. N. J.; Curtis, B. J. B. J.; Hang, M. N. M. N.; Gallagher, M. J. M. J.; Fairbrother, D. H. H.; Hamers, R. J. R. J.; Klaper, R. D. R. D. Next-Generation Complex Metal Oxide Nanomaterials Negatively Impact Growth and Development in the Benthic Invertebrate *ChironomusrRiparius* upon Settling. *Environ. Sci. Technol.* **2019**, *53* (7), 3860–3870. https://doi.org/10.1021/acs.est.8b06804.

(28) Bozich, J.; Hang, M.; Hamers, R.; Klaper, R. Core Chemistry Influences the Toxicity of Multicomponent Metal Oxide Nanomaterials, Lithium Nickel Manganese Cobalt Oxide,

and Lithium Cobalt Oxide to *Daphnia magna*. *Environ. Toxicol. Chem.* **2017**, *36* (9), 2493–2502. https://doi.org/10.1002/etc.3791.

(29) Martins, J.; Oliva Teles, L.; Vasconcelos, V. Assays with *Daphnia magna* and *Danio rerio* as Alert Systems in Aquatic Toxicology. *Environ. Int.* **2007**, *33* (3), 414–425. https://doi.org/10.1016/j.envint.2006.12.006.

(30) Niemuth, N. J.; Zhang, Y.; Mohaimani, A. A.; Schmoldt, A.; Laudadio, E. D.; Hamers, R. J.; Klaper, R. D. Protein Fe–S Centers as a Molecular Target of Toxicity of a Complex Transition Metal Oxide Nanomaterial with Downstream Impacts on Metabolism and Growth. *Environ. Sci. Technol.* **2020**, *54* (23), 15257–15266. https://doi.org/10.1021/acs.est.0c04779.

(31) Laudadio, E. D.; Bennett, J. W.; Green, C. M.; Mason, S. E.; Hamers, R. J. Impact of Phosphate Adsorption on Complex Cobalt Oxide Nanoparticle Dispersibility in Aqueous Media. *Environ. Sci. Technol.* **2018**, *52* (17), 10186–10195. https://doi.org/10.1021/acs.est.8b02324.

(32) Andrews, S.; Krueger, F.; Seconds-Pichon, A.; Biggins, F.; Wingett, S. FastQC: A Quality Control Tool for High Throughput Sequence Data; *Babraham Bioinformatics*, Babraham Institute, Cambridge, United Kingdom, 2010; Vol. 1, p 1.

(33) Martin, M. Cutadapt Removes Adapter Sequences from High-Throughput Sequencing Reads. *EMBnet.journal* **2011**, *17* (1), 10. https://doi.org/10.14806/ej.17.1.200.

(34) Bray, N. L.; Pimentel, H.; Melsted, P.; Pachter, L. Near-Optimal Probabilistic RNA-Seq Quantification. *Nat. Biotechnol.* **2016**, *34* (5), 525–527. https://doi.org/10.1038/nbt.3519.

(35) Love, M. I.; Huber, W.; Anders, S. Moderated Estimation of Fold Change and Dispersion for RNA-Seq Data with DESeq2. *Genome Biol.* **2014**, *15* (12), 550. https://doi.org/10.1186/s13059-014-0550-8.

(36) Camacho, C.; Coulouris, G.; Avagyan, V.; Ma, N.; Papadopoulos, J.; Bealer, K.; Madden, T. L. BLAST+: Architecture and Applications. *BMC Bioinformatics* **2009**, *10* (1), 421. https://doi.org/10.1186/1471-2105-10-421.

(37) Yoo, A. B.; Jette, M. A.; Grondona, M. SLURM: Simple Linux Utility for Resource Management; 2003; pp 44–60. https://doi.org/10.1007/10968987_3.

(38) Tange, O. Gnu Parallel-the Command-Line Power Tool. *USENIX Mag.* **2011**, *36* (1), 42–47.

(39) Huang, D. W.; Sherman, B. T.; Lempicki, R. A. Systematic and Integrative Analysis of Large Gene Lists Using DAVID Bioinformatics Resources. *Nat. Protoc.* **2009**, *4* (1), 44–57. https://doi.org/10.1038/nprot.2008.211.

(40) Huang, D. W.; Sherman, B. T.; Lempicki, R. A. Bioinformatics Enrichment Tools: Paths toward the Comprehensive Functional Analysis of Large Gene Lists. *Nucleic Acids Res.* **2009**, *37* (1), 1–13. https://doi.org/10.1093/nar/gkn923.

(41) Kanehisa, M.; Goto, S. KEGG: Kyoto Encyclopedia of Genes and Genomes. *Nucleic Acids Res.* **2000**, *28* (1), 27–30. https://doi.org/10.1093/nar/28.1.27.

(42) Kanehisa, M.; Sato, Y.; Furumichi, M.; Morishima, K.; Tanabe, M. New Approach for Understanding Genome Variations in KEGG. *Nucleic Acids Res.* **2019**, *47* (D1), D590–D595. https://doi.org/10.1093/nar/gky962.

(43) Kanehisa, M. Toward Understanding the Origin and Evolution of Cellular Organisms. *Protein Sci.* **2019**, *28* (11), 1947–1951. https://doi.org/10.1002/pro.3715.

(44) Taylor, N. S.; Weber, R. J. M.; Southam, A. D.; Payne, T. G.; Hrydziuszko, O.; Arvanitis, T. N.; Viant, M. R. A New Approach to Toxicity Testing in *Daphnia magna*: Application of High Throughput FT-ICR Mass Spectrometry Metabolomics. *Metabolomics* **2009**, *5* (1), 44–58. https://doi.org/10.1007/s11306-008-0133-3.

(45) Davidson, R. L.; Weber, R. J. M.; Liu, H.; Sharma-Oates, A.; Viant, M. R. Galaxy-M: A Galaxy Workflow for Processing and Analyzing Direct Infusion and Liquid Chromatography Mass Spectrometry-Based Metabolomics Data. *Gigascience* **2016**, *5* (1), 10. https://doi.org/10.1186/s13742-016-0115-8.

(46) Xia, J.; Psychogios, N.; Young, N.; Wishart, D. S. MetaboAnalyst: A Web Server for Metabolomic Data Analysis and Interpretation. *Nucleic Acids Res.* **2009**, *37* (Web Server), W652–W660. https://doi.org/10.1093/nar/gkp356.

(47) Efremov, R. G.; Baradaran, R.; Sazanov, L. A. The Architecture of Respiratory Complex I. *Nature* **2010**, *465* (7297), 441–445. https://doi.org/10.1038/nature09066.

(48) Mensch, A. C.; Mitchell, H. D.; Markillie, L. M.; Laudadio, E. D.; Hedlund Orbeck, J. K.; Dohnalkova, A.; Schwartz, M. P.; Hamers, R. J.; Orr, G. Subtoxic Dose of Lithium Cobalt Oxide Nanosheets Impacts Critical Molecular Pathways in Trout Gill Epithelial Cells. *Environ. Sci. Nano* **2020**, *7* (11), 3419–3430. https://doi.org/10.1039/D0EN00844C.

(49) Futai, M.; Sun-Wada, G.-H.; Wada, Y.; Matsumoto, N.; Nakanishi-Matsui, M. Vacuolar-Type ATPase: A Proton Pump to Lysosomal Trafficking. *Proc. Japan Acad. Ser. B* **2019**, *95* (6), 261–277. https://doi.org/10.2183/pjab.95.018.

(50) Bareth, B.; Dennerlein, S.; Mick, D. U.; Nikolov, M.; Urlaub, H.; Rehling, P. The Heme a Synthase Cox15 Associates with Cytochrome c Oxidase Assembly Intermediates during Cox1 Maturation. *Mol. Cell. Biol.* **2013**, *33* (20), 4128–4137. https://doi.org/10.1128/MCB.00747-13.

(51) Banci, L.; Bertini, I.; Ciofi-Baffoni, S.; Hadjiloi, T.; Martinelli, M.; Palumaa, P. Mitochondrial Copper(I) Transfer from Cox17 to Sco1 Is Coupled to Electron Transfer. *Proc. Natl. Acad. Sci.* **2008**, *105* (19), 6803–6808. https://doi.org/10.1073/pnas.0800019105.

(52) Pagano, L.; Maestri, E.; Caldara, M.; White, J. C.; Marmiroli, N.; Marmiroli, M. Engineered Nanomaterial Activity at the Organelle Level: Impacts on the Chloroplasts and Mitochondria. *ACS Sustain. Chem. Eng.* **2018**, *6* (10), 12562–12579. https://doi.org/10.1021/acssuschemeng.8b02046.

(53) Wang, K.; Wan, J.; Xiang, Y.; Zhu, J.; Leng, Q.; Wang, M.; Xu, L.; Yang, Y. Recent Advances and Historical Developments of High Voltage Lithium Cobalt Oxide Materials for Rechargeable Li-Ion Batteries. *J. Power Sources* **2020**, *460*, 228062. https://doi.org/10.1016/j.jpowsour.2020.228062.

(54) G, H.; S, S.; P, G.; Shrivash, M. K.; Kumar, D. Synthesis of Chromium Doped Cobalt Oxide (Cr:Co_3O_4) Nanoparticles by Co-Precipitation Method and Enhanced Photocatalytic Properties in the Visible Region. *J. Mater. Sci. Eng.* **2018**, *07* (01). https://doi.org/10.4172/2169-0022.1000419.

(55) Melby, E. S.; Cui, Y.; Borgatta, J.; Mensch, A. C.; Hang, M. N.; Chrisler, W. B.; Dohnalkova, A.; Van Gilder, J. M.; Alvarez, C. M.; Smith, J. N.; Hamers, R. J.; Orr, G.

Impact of Lithiated Cobalt Oxide and Phosphate Nanoparticles on Rainbow Trout Gill Epithelial Cells. *Nanotoxicology* **2018**, *12* (10), 1166–1181. https://doi.org/10.1080/17435390.2018.1508785.

(56) Peregrín-Alvarez, J. M.; Sanford, C.; Parkinson, J. The Conservation and Evolutionary Modularity of Metabolism. *Genome Biol.* **2009**, *10* (6), R63. https://doi.org/10.1186/gb-2009-10-6-r63.

Figures

Table 1. Selected DAVID enrichment terms for differentially expressed genes between lithium cobalt oxide 1 mg/L and control.

Category	Term	Gene count	Benjamini-adjusted p-value
Energy metabolism			
GO: Cellular component	Mitochondrial respiratory chain complex I	17	0.0002
UniProt keyword	Ubiquinone	16	0.0004
UniProt keyword	Oxidoreductase	80	0.0006
GO: Cellular component	Plasma membrane proton-transporting V-type ATPase complex	13	0.002
GO: Biological process	Cellular response to starvation	25	0.002
GO: Cellular component	Mitochondrion	70	0.004
UniProt keyword	ATP-binding	70	0.006
KEGG pathway	Oxidative phosphorylation	53	0.01
GO: Molecular function	NADH dehydrogenase activity	12	0.05
GO: Molecular function	NADH dehydrogenase (ubiquinone) activity	13	0.05
GO: Biological process	ATP hydrolysis coupled proton transport	18	0.06
GO: Biological process	Mitochondrial electron transport, NADH to ubiquinone	12	0.06
UniProt keyword	One-carbon metabolism	5	0.07
Proteins and amino acids			
UniProt keyword	Ribosome biogenesis	21	0.0009
UniProt keyword	Protein biosynthesis	40	0.003
UniProt keyword	Aminoacyl-tRNA synthetase	20	0.003
KEGG pathway	Ribosome biogenesis in eukaryotes	38	0.01
KEGG pathway	Protein export	17	0.01
UniProt keyword	Protease	86	0.02
KEGG pathway	Aminoacyl-tRNA biosynthesis	25	0.08
GO: Biological process	rRNA processing	13	0.08

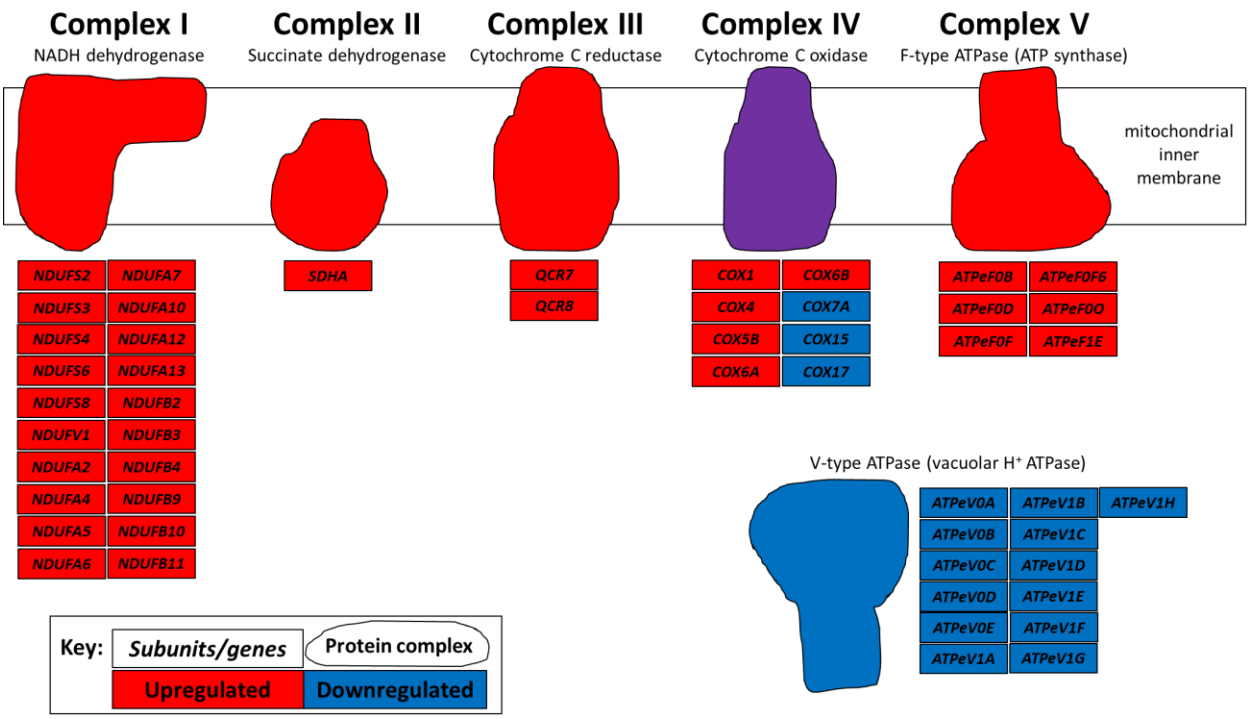

Figure 1. Diagram of oxidative phosphorylation showing genes differentially expressed between lithium cobalt oxide 1 mg/L and control.

Table 2. MetaboAnalyst enriched KEGG pathways for differential metabolites between lithium cobalt oxide 1 mg/L and control.

KEGG pathway	Gamma-adjusted p-value	KEGG ID	Putatively annotated metabolites
Histidine metabolism	0.02	C00386, C00135, C01262	Carnosine; L-Histidine; beta-Alanyl-N(pi)-methyl-L-histidine
beta-Alanine metabolism	0.03	C01013, C00429, C00386, C00135	3-Hydroxypropanoate; 5,6-Dihydrouracil; Carnosine; L-Histidine
Starch and sucrose metabolism	0.03	C00089, C01083, C00208, C00721	Sucrose; alpha,alpha-Trehalose; Maltose; Dextrin
Valine leucine and isoleucine biosynthesis	0.03	C00123, C00407, C00183	L-Leucine; L-Isoleucine; L-Valine
Glycerophospholipid metabolism	0.04	C00588, C00114, C01996, C01233	Choline phosphate; Choline; Acetylcholine; sn-Glycero-3-phosphoethanolamine
Insect hormone biosynthesis	0.04	C00448, C03461	trans,trans-Farnesyl diphosphate; 2-trans,6-trans-Farnesal
Galactose metabolism	0.04	C05404, C00089, C00492, C05402, C05400, C01235, C00243	D-Gal alpha; Sucrose; Raffinose; Melibiose; Epimelibiose; alpha-D-Galactosyl-(1->3)-1D-myo-inositol; Lactose
Aminoacyl-tRNA biosynthesis	0.04	C00135, C00183, C00407, C00123, C00148, C01110	L-Histidine; L-Valine; L-Isoleucine; L-Leucine; L-Proline; 5-Amino-2-oxopentanoic acid
D-Arginine and D-ornithine metabolism	0.05	C01110, C03771	5-Amino-2-oxopentanoic acid; 5-Guanidino-2-oxopentanoate
Tryptophan metabolism	0.05	C00643, C05648, C05639, C01252, C05637, C05635, C00448	5-Hydroxy-L-tryptophan; 5-Hydroxy-N-formylkynurenine; 4,6-Dihydroxyquinoline; 4-(2-Aminophenyl)-2,4-dioxobutanoate; 4,8-Dihydroxyquinoline; 5-Hydroxyindoleacetate; trans,trans-Farnesyl diphosphate
Terpenoid backbone biosynthesis	0.06	C00448, C03461	trans,trans-Farnesyl diphosphate; 2-trans,6-trans-Farnesal
Valine leucine and isoleucine degradation	0.07	C00183, C00407, C00123	L-Valine; L-Isoleucine; L-Leucine
Glycine serine and threonine metabolism	0.08	C00114, C00719, C00430	Choline; Betaine; 5-Aminolevulinate

Lysine degradation	0.08	C01181, C00449	4-Trimethylammoniobutanoate; N6-(L-1,3-Dicarboxypropyl)-L-lysine
Pantothenate and CoA biosynthesis	0.09	C00429, C00183	5,6-Dihydrouracil; L-Valine
Arginine and proline metabolism	0.09	C00763, C00148, C03440, C01165, C05945, C00884, C01157	D-Proline; L-Proline; cis-4-Hydroxy-D-proline; L-Glutamate 5-semialdehyde; L-Arginine phosphate; Homocarnosine; Hydroxyproline

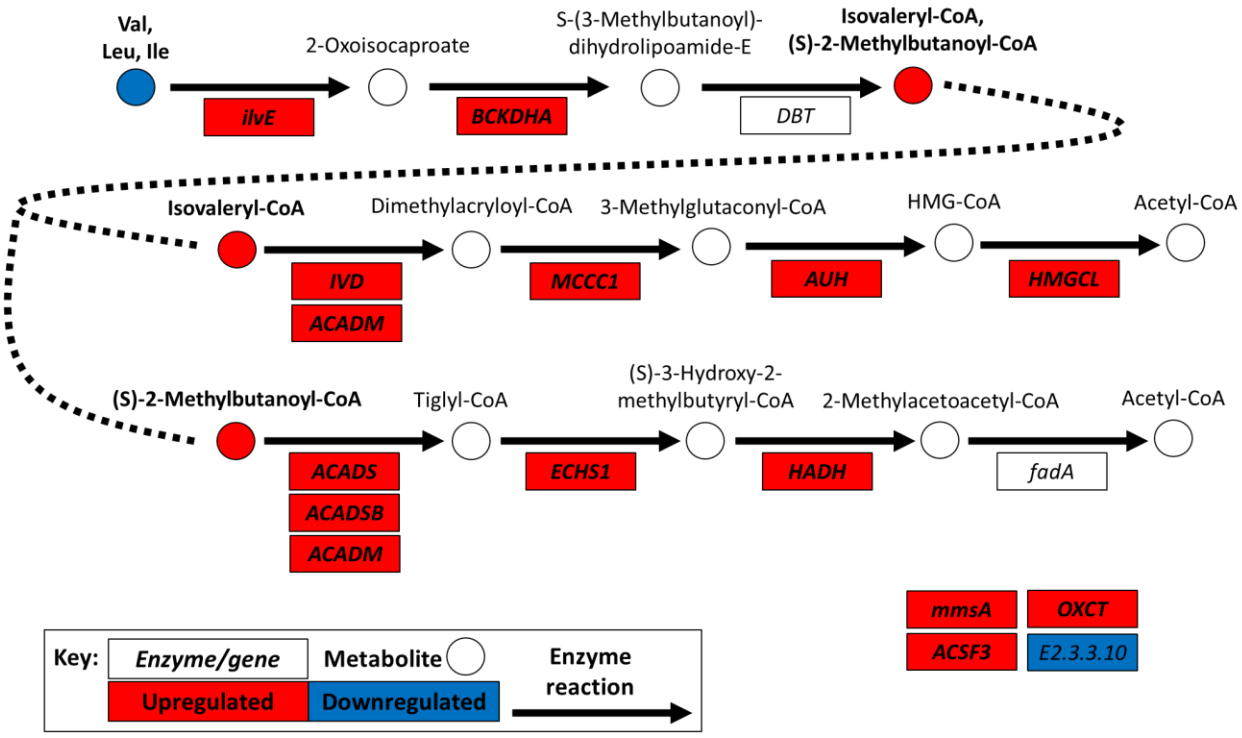

Figure 2. Pathway for valine, leucine, and isoleucine degradation showing differential putatively annotated metabolites and genes between LCO 1 mg/L and control.

Table 3. Differential sugars in Starch, Sucrose, and Galactose metabolism identified by Metaboanalyst between lithium cobalt oxide 1 mg/L and control.

m/z	Matched ion form	KEGG compound	Putatively annotated metabolite	Fold change	FDR-adjusted p-value
342.11202	M(C13)-H[-]	C00089, C00185, C00208, C00243, C00252, C01083, C01235, C05400, C05402	Sucrose, Cellobiose, Maltose, Lactose, Isomaltose, Trehalose, Galactinol, Epimelibiose, Melibiose	1.5	0.08
377.08558	M+Cl[-]	C00089, C00185, C00208, C00243, C00252, C01083, C01235, C05400, C05402	Sucrose, Cellobiose, Maltose, Lactose, Isomaltose , Trehalose, Galactinol, Epimelibiose, Melibiose	2.3	0.024
379.08258	M+Cl37[-]	C00089, C00185, C00208, C00243, C00252, C01083, C01235, C05400, C05402	Sucrose, Cellobiose, Maltose, Lactose, Isomaltose, Trehalose, Galctinol, Epimelibiose, Melibiose	2.2	0.03
503.16200	M-H[-]	C00492, C00721, C05404	Raffinose, Dextrin, Manninotriose	1.03	0.008
527.15958	M+Na[1+]	C00492, C00721, C05404	Raffinose, Dextrin, Manninotriose	2.2	0.01
539.13874	M+Cl[-]	C00492, C00721, C05404	Raffinose, Dextrin, Manninotriose	1.03	0.009
563.18265	M+CH3COO[-]	C00492, C00721, C05404	Raffinose, Dextrin, Manninotriose	1.03	0.004

Figure Legends

Figure 1. Diagram of oxidative phosphorylation showing genes differentially expressed between lithium cobalt oxide 1 mg/L and control. Diagram of oxidative phosphorylation, based on KEGG map 00190, showing genes differentially expressed (FDR-adjusted $p < 0.1$) between lithium cobalt oxide 1 mg/L exposed and control daphnids at 48 h. Upregulated genes include: Complex I genes NADH dehydrogenase Fe-S proteins (*NDUFS*) *2*, *3*, *4*, *6*, and *8*, NADH dehydrogenase flavoprotein 1 (*NDUFV1*), NADH dehydrogenase 1 alpha subcomplex (*NDUFA*) subunits *2*, *4*, *5*, *6*, *7*, *10*, *12*, and *13*, and NADH dehydrogenase 1 beta (*NDUFB*) subunits *2*, *3*, *4*, *9*, *10*, and *11*; Complex II gene succinate dehydrogenase flavoprotein subunit (*SDHA*); Complex III genes ubiquinol-cytochrome c reductase (*QCR*) subunits *7* and *8*; Complex IV genes cytochrome c oxidase (*COX*) subunits *1*, *4*, *5B*, *6A*, and *6B*; and Complex V genes F-type H^+-transporting ATPase (*ATPeF0*) subunits *B*, *D*, *F*, *F6*, and *O*, and F-type H^+-transporting ATPase subunit epsilon (*ATPeF1E*). This coordinated upregulation supports compensation for energy starvation. Downregulated genes include: Complex IV genes heme a synthase (*COX15*), involved synthesis of heme a, cytochrome c oxidase assembly protein subunit 17 (*COX17*), involved in transfer of copper, and cytochrome c oxidase subunit 7a (*COX7A*). Downregulation of *COX15* and *COX17* support disruption of heme synthesis and metal homeostasis by LCO exposure. Also downregulated are subunits of the V-type H^+-transporting ATPase (*ATPeV*) localized to the vacuole, which uses ATP to pump protons into the vacuole: *0A*, *0B*, *0C*, *0D*, *0E*, *1A*, *1B*, *1C*, *1D*, *1E*, *1F*, *1G*, and *1H*. Downregulation of this ATP-using complex suggests downregulation of ATP-using processes for energy conservation.

Figure 2. Pathway for Valine, leucine, and isoleucine degradation showing differential compounds and genes between lithium cobalt oxide 1 mg/L and control. Diagram of valine, leucine, and isoleucine degradation based on KEGG map 00280, showing metabolites and genes significantly different (FDR-adjusted $p < 0.1$) between lithium cobalt oxide 1 mg/L exposed and control daphnids at 48 h. Putatively annotated amino acids valine (Val), leucine (Leu), and isoleucine (Ile) are significantly lower in 1 mg/L exposed daphnids than in controls, while the intermediate metabolites of Leu and Ile breakdown, isoveryl-CoA and (S)-2-Methylbutanoyl-CoA are both significantly increased, pointing to breakdown on these amino acids. Upregulated genes involved in Val, Leu, and Ile breakdown are, in order of appearance in the highlighted pathway: branched-chain amino acid aminotransferase (*ilvE*), 2-oxoisovalerate dehydrogenase E1 component alpha subunit (*BCKDHA*), isovaleryl-CoA dehydrogenase (*IVD*), acyl-CoA dehydrogenase (*ACADM*), 3-methylcrotonyl-CoA carboxylase alpha subunit (*MCCC1*), methylglutaconyl-CoA hydratase (*AUH*), hydroxymethylglutaryl-CoA lyase (*HMGCL*), butyryl-CoA dehydrogenase (*ACADS*), short-chain 2-methylacyl-CoA dehydrogenase (*ACADSB*), enoyl-CoA hydratase (*ECHS1*), and 3-hydroxyacyl-CoA dehydrogenase (*HADH*). Not significantly changed genes in the highlighted pathway are: dihydrolipoyl transacylase (*DBT*) and acetyl-CoA acyltransferase (*fadA*). Ancillary genes included in KEGG map 00280 that were upregulated are: methylmalonate-semialdehyde dehydrogenase (*mmsA*), 3-oxoacid CoA-transferase (*OXCT*), and malonyl-CoA/methylmalonyl-CoA synthetase (*ACSF3*). Ancillary gene hydroxymethylglutaryl-CoA synthase (*E2.3.3.10*) was downregulated. Taken together, metabolite and gene expression changes support amino acid breakdown as a means to compensate for energy starvation, by increasing production of Acetyl-CoA for the citric acid cycle.